Temperature effects on the structure and dynamics of liquid dimethyl sulfoxide: A molecular dynamics study

ARTICLE *in* FLUID PHASE EQUILIBRIA · MAY 2008

Impact Factor: 2.2 · DOI: 10.1016/j.fluid.2008.02.019

3 AUTHORS:

Michail Chalaris
Hellenic Fire Academy, Kifisia, Greece
29 PUBLICATIONS **281** CITATIONS
SEE PROFILE

S. Marinakis
Queen Mary, University of London
26 PUBLICATIONS **418** CITATIONS
SEE PROFILE

Dimitris Dellis
National and Kapodistrian University of Ath…
15 PUBLICATIONS **179** CITATIONS
SEE PROFILE

Fluid Phase Equilibria 267 (2008) 47–60

Contents lists available at ScienceDirect

Fluid Phase Equilibria

journal homepage: www.elsevier.com/locate/fluid

Temperature effects on the structure and dynamics of liquid dimethyl sulfoxide: A molecular dynamics study

Michail Chalaris [1], Sarantos Marinakis [a,*], Dimitris Dellis [b]

[a] School of Engineering and Physical Sciences, Heriot-Watt University, William Perkin Building, Edinburgh EH14 4AS, UK
[b] Laboratory of Physical Chemistry, Department of Chemistry, University of Athens, Panepistimiopolis, 15771 Athens, Greece

ARTICLE INFO

Article history:
Received 7 January 2008
Received in revised form 14 February 2008
Accepted 18 February 2008
Available online 23 February 2008

Keywords:
DMSO
Dimethyl sulfoxide
Computer simulation
Molecular dynamics
Transport coefficients
Diffusion
Shear viscosity
Dielectric properties
Microscopic structure
Thermodynamic properties
Stokes–Einstein–Debye relation
Dipole relaxation times
Glarum–Powles model
Fatuzzo–Mason model

ABSTRACT

The molecular dynamics (MD) simulation technique has been employed to investigate the thermodynamic properties and transport coefficients of the neat liquid dimethyl sulfoxide (DMSO). The fluid has been studied at temperatures in the range 298–353 K and at a pressure equal to 1 atm. The simulations employed a nine-site potential model, which is presented for the first time here, and all the available non-polarizable models. The performance of each model is tested using the same statistical mechanical ensemble and simulation method under the same conditions, revealing its weaknesses and strengths. Thermodynamic properties, microscopic structure and dynamic properties, such as transport coefficients, rotational and single-dipole correlation times have been calculated and compared with available experimental results. Estimations of transport coefficients from various theoretical and empirical models are tested against experimental and MD results. Translational and rotational dynamics suggest the existence of the cage effect and agree with the Stokes–Einstein–Debye relation. The dipole relaxation times calculated are discussed in terms of simple and useful approximations, such as the Glarum–Powles and Fatuzzo–Mason models.

1. Introduction

Dimethyl sulfoxide (DMSO) is one of the most interesting aprotic organic solvents because of its unique physicochemical properties, such as the high normal boiling point (189 °C), and the extremely high values of its dipole moment (3.96 ± 0.04 D [1]) and its dielectric constant (47.24 at 20 °C [2]). Because of these properties, DMSO has been an indispensable tool in organic synthesis [3] and it has been widely used as a cryoprotectant and radioprotectant in many applications in pharmacological industry [4]. Despite the presence of two hydrophobic methyl groups, DMSO favors the formation of hydrogen bonds with water molecules, resulting in mixtures with interesting, strong non-ideal behavior [5,6]. These unique properties attracted much experimental interest and a rich variety of experimental techniques, such as neutron and X-ray scattering [7–10], Infra-red absorption and Raman scattering [11,12], nuclear magnetic resonance [13,14], acoustic and dielectric measurements [15–17], mass spectroscopy [18], time-resolved Kerr [19] and fluorescence upconversion spectroscopy [20] have been used for its study. Despite this wealth of experimental data, there are still relatively few studies concerning the transport coefficients [21–28] and there still exists a disagreement between experimental [6] and theoretical studies on the microscopic structure of DMSO.

On the theoretical side, ab initio calculations have been carried out to study pure DMSO and its clusters with some adducts, and especially water molecules [5,29–31]. Molecular dynamics (MD) [32] computer simulations have been proved to be an indispensable tool for the elucidation of many properties in the liquid and gas phase and the first MD study on the DMSO properties was reported by Rao and Singh [33]. In that study, the authors proposed a four-site pairwise effective potential model (RS) and obtained information on free energies of solvation and the microscopic structure of ionic solutions of DMSO. Then, Luzar, Soper and Chandler [6,34,35] performed a combined neutron diffraction and MD study of liquid DMSO at room temperature employing two new model

* Corresponding author. Tel.: +44 131 451 4113; fax: +44 131 451 3180.
E-mail addresses: mchalaris@chem.uoa.gr (M. Chalaris), S.Marinakis@hw.ac.uk (S. Marinakis), ntell@chem.uoa.gr (D. Dellis).
[1] Present address: Hellenic Fire Corps Headquarters, Direction of Health and Safety, 31 Piraeos Str., 10553 Athens, Greece.

0378-3812/$ – see front matter © 2008 Elsevier B.V. All rights reserved.
doi:10.1016/j.fluid.2008.02.019

Table 1
Force field parameters of various models for DMSO[a]

	RS	P1	P2	VG	Bordat	OPLS	NPS	GOVG	JM4[b]	JM9[c]
ε_{OO}/k_B (K)	33.21	35.99	35.99	206.32	206.32	140.86	71.06	206.32[d]	185.0	31.00
σ_{OO} (Å)	2.94	2.80	2.80	2.63	2.63	2.93	2.92	2.63[d]	2.920	2.94
q_O (e)	−0.459	−0.54	−0.459	−0.459	−0.43674	−0.459	−0.459	−0.44753	−0.459	−0.5205
ε_{SS}/k_B (K)	101.65	119.96	119.96	156.00	155.99	198.71	168.18	156.02[d]	139.0	98.00
σ_{SS} (Å)	3.56	3.40	3.40	3.56	3.56	3.56	3.66	3.56[d]	3.60	0.3560
q_S (e)	0.139	0.54	0.139	0.139	0.11674	0.139	0.139	0.12753	0.139	0.3155
ε_{CC}/k_B (K)	80.58	147.94	147.94	113.23	113.23	80.49	11.51	104.30[d]	98.95	75.00
σ_{CC} (Å)	3.60	3.00	3.80	3.66	3.739	3.81	3.76	3.748[d]	3.80	3.70
q_C (e)	0.160	0.00	0.160	0.160	0.16	0.160	0.160	0.1600	0.160	−0.3244
μ (D)	4.48	3.97	4.48	4.59	4.39	4.48	4.48	5.25	4.41	4.6512

[a] Molecular geometries (rigid) of the models. RS, P1, P2, OPLS, NPS models: r_{OS} = 1.53 Å, r_{SC} = 1.80 Å, ∠OSC = 106.75°, ∠CSC = 97.4°, for the VG, Bordat models, the value of the r_{SC} is 1.95 Å, and for the GOVG model, r_{SC} = 1.937991 Å.

[b] For the JM4 model: r_{OS} = 1.496 Å, r_{SC} = 1.805 Å, ∠OSC = 107.0°, ∠CSC = 100.4°.

[c] In the JM9 model the C, and the three H atoms are considered independently, and r_{OS} = 1.49579 Å, r_{SC} = 1.80468 Å, r_{CH} = 1.07996 Å, ∠OSC = 106.75°, ∠CSC = 97.42°. The same geometry was used for the deuterated case.

[d] Calculated from the C_6 and C_{12} values (presented in Table 2 in Ref. [42]).

potentials, the so-called P1 and P2 [36]. In an attempt to refine these models, Liu et al. presented a new computational model (VG) [35] based on the parameters of the previous models and the GROMOS force field [37]. The force field of this model was reparameterized by Bordat et al. [38] resulting in a new potential model, which is usually referred as Bordat's model. Zheng and Ornstein [39] used a new model (OPLS), which was constructed by Jorgensen [40], to study the effects of DMSO on enzyme structures and dynamics. All the above-mentioned models are rigid and non-polarizable, and use four interaction sites to describe the sulfur atom, the oxygen atom and the two methyl groups. In order to describe better the intermolecular potential, these models employ both short-range Lennard–Jones and long-range coulombic terms (see Table 1). A new, rigid model was presented by Vishnyakov et al. [41] and was used to calculate thermodynamic, structural and dynamical properties at T = 303 K. Geerke et al. [42] improved the VG model and constructed the latest available model, which we will refer to as GOVG hereafter. This model was used for a multiproperty study of the neat liquid DMSO at temperatures T = 298 and 303 K and at pressure P = 1 atm. In addition to these models, non-rigid models also exist [43–46], but we do not include them in the current study because of the excessive computational time they require.

It should be noted that each model accurately reproduces some properties but fails systematically in others. Almost all the previously published calculations have been carried out either at T = 298 or 303 K. In order to compare the performance of all these models with the available experimental data at various thermodynamic conditions, the present work covers a considerably wider temperature range from 298 K to 353 K. In addition to this, we have included in our calculations two potential models constructed by us. The first model [47] treats DMSO molecules with four interaction sites: The S and O atoms and the two methyl groups, with the latter being considered as united atoms. The second model, presented here for the first time, employs nine interaction sites, taking into account each atom separately in an all-atom model. We derived these models using quantum mechanical methods to initially optimize the molecular structure, then fit partial charges to quantum mechanical electrostatic potential, and then we adjusted the van der Waals parameters so as to reproduce as much as possible the experimental data. A particular reason to use the computationally more expensive nine-site model was to investigate whether an all-atom model could close the gap between experimental and theoretical results on the liquid structure [41].

The strengths and weaknesses of all the available models are discussed in the view of their ability to reproduce various properties such as the potential energy and pressure, the microscopic structure, the diffusion coefficient and shear viscosity, and the rotational–reorientational correlation times. In addition to this, the fully deuterated dimethyl sulfoxide (DMSO-*d*6) has been studied at liquid conditions at various temperatures. For the study of DMSO-*d*6, a particular emphasis is given to the transport coefficients, and the isotopic dependence of the dynamical properties is also discussed. The outline of the paper is as follows. The newly optimized intermolecular potentials, and the relevant computational details are presented in Section 2. In Section 3, the results from the new models are presented and compared alongside those obtained using previous potential models. In the same section, various empirical models and theoretical predictions are included to provide further insight into the simulations results, while Section 4 summarizes our main conclusions.

2. Computational aspects: molecular models and simulation details

The models employed in this study have used a number of assumptions. The DMSO molecule was treated as a rigid moiety, with fixed bond lengths and angles (see Fig. 1). For the new derived models, the unoptimized geometry was taken from X-ray diffraction data [48,49] and the partial charges were taken from ab initio calculations [33]. Pairwise additive potential functions were used to describe the potential between the various interaction sites, while polarizability and many-body interactions were neglected. Thus, the intermolecular pair-potential can be written as a sum of the long-range electrostatic and the short-range Lennard–Jones (12–6) interaction terms:

$$U_{ab}(r) = \frac{q_a q_b}{r} + 4\varepsilon_{ab}\left[\left(\frac{\sigma_{ab}}{r}\right)^{12} - \left(\frac{\sigma_{ab}}{r}\right)^{6}\right] \quad (1)$$

In Eq. (1), r represents the distance between the sites a and b, q_a and q_b are the partial charges and ε and σ are the optimized Lennard–Jones coefficients. The optimized coefficients were obtained after many trial simulation runs evaluating their performance in reproducing thermodynamical and dynamical properties. In all cases the Lennard–Jones parameters between interaction sites of different types are described by the commonly applied Lorentz–Berthelot combination rules: $\varepsilon_{ab} = (\varepsilon_{aa}\varepsilon_{bb})^{1/2}$, $\sigma_{ab} = 0.5(\sigma_{aa} + \sigma_{bb})$. The interaction coefficients obtained in the present work along with the ones from previous studies are shown together in Table 1.

Most of the MD simulations described here were carried out using the NVE statistical mechanical ensemble, although few have been done in the NVT ensemble (see Table 2). In each MD run, a face-centered cubic initial configuration was employed. The initial

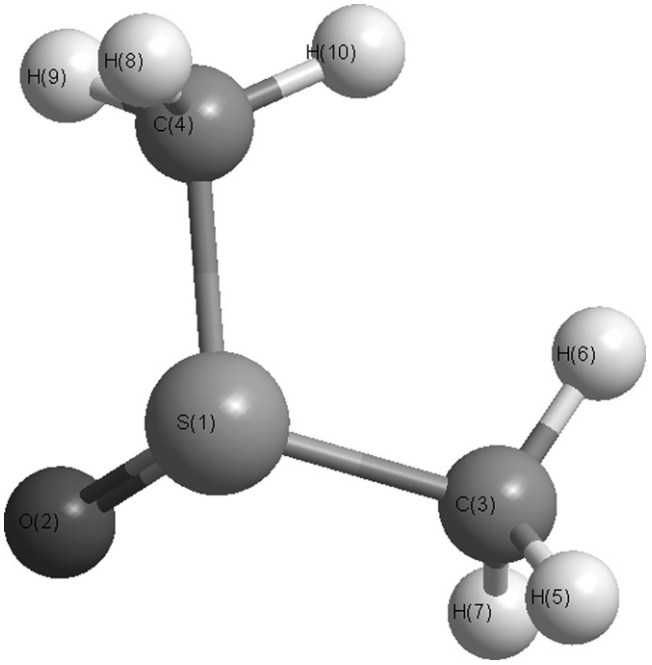

Fig. 1. Bond distances and angles of the DMSO JM9 model geometry employed in this study: r_{OS} = 1.49579 Å, r_{SC} = 1.80468 Å, r_{CH} = 1.07996 Å, ∠OSC = 106.75°, ∠CSC = 97.42°. For the JM4 model r_{OS} = 1.496 Å, r_{SC} = 1.805 Å, ∠OSC = 107.0°, ∠CSC = 100.4°. See text for details.

random linear velocities of the species were selected from a Gaussian distribution, which could model the required thermal motion of the atoms at the temperatures of interest. In all simulations, a full cut-off radius ($r_c = L_{box}/2$) was used, where L_{box} is the length of the simulation box and the long-range electrostatic interactions have been computed using the Ewald sum method with conducting boundaries [32], as in previous studies from our group [50–52]. The total number of molecules in the simulation box was 500 in all cases. Simulations employing higher number of molecules have also been carried out and only small, non-systematic differences were observed. In order to melt the lattice and attain thermal equilibration, an initial run of 100,000 steps was carried out. The equation of motion was integrated using the leapfrog modification of the Verlet algorithm [32] with a time step of 1 fs, and the number of steps for the production run was between 100,000 and 300,000 for the various thermodynamic states.

The self-diffusion coefficients were calculated from the Einstein equation [32]:

$$D = \lim_{t\to\infty} \frac{\langle |r_i(t) - r_i(0)|^2 \rangle}{6t},$$

where $r_i(t)$ is the position of particle i at time t and, $\langle \dots \rangle$ denotes the time average. In this approach, D is obtained from the linear region of the mean squared displacement (MSD) versus t. This method is preferred over the use of velocity autocorrelation functions [53,54]. It has been established that relatively long MSD plots of tens of picosecond are necessary to obtain reliable results. In the present study, MSD plots of 400 ps were produced and only the last 150 ps were taken into account in the calculation of the self-diffusion coefficient. In addition, the shear viscosity of the liquids was also calculated for the DMSO-*d*0 at various temperatures, and for DMSO-*d*6 at a temperature of 298 K. The shear viscosity was calculated using the following Green–Kubo equation:

$$\eta = \frac{V}{k_B T} \int_0^\infty \langle P_{\alpha\beta}(0) P_{\alpha\beta}(t) \rangle \, dt,$$

with $\alpha\beta = xy, xz, yz$ and

$$P_{\alpha\beta} = \frac{1}{V} \left[\sum_V \sum_{i=1}^{N_V} m_V \left(\frac{p_{\alpha i}}{m_V} - \upsilon_\alpha \right) \left(\frac{p_{\alpha i}}{m_V} - \upsilon_\beta \right) - \sum_{i=1}^{N-1} \sum_{j>1}^{N} \left(\frac{r_{\alpha ij} r_{\beta ij}}{\vec{r}_{ij}} \right) \frac{dU(r_{ij})}{dr} \right] \quad (2)$$

In Eq. (2), V is the volume of the simulation box, and $p_{\alpha i}$ is the α-component of the momentum of particle i. The simulations for these calculations had a time length of 1.2 ns. During the simulation and at every five time steps the off-diagonal $P_{\alpha\beta}$ ($\alpha \neq \beta$) of the pressure tensor P were saved. The statistical precision of the shear viscosity is worse than that of the self-diffusion coefficient because the latter is a single-particle property which can be averaged over the N identical particles that comprise the simulation box [32]. For this reason, only the averaged values over different components, $\alpha,\beta = xy, yz, zx$ of $P_{\alpha\beta}$ are presented in Section 3.

In order to obtain information about the translational dynamics, one needs the autocorrelation functions [32] of the center-of-mass linear velocity, VACF or $C_{VV}(t)$, and of the total force, FACF or $C_{FF}(t)$. For the description of the rotational dynamics, the torque, $C_{TT}(t)$, and the angular momentum autocorrelation functions, $C_{JJ}(t)$, have been calculated. The first, and second rank Legendre (P_1 and P_2, respectively) reorientation correlation functions $C_{1,2}(t) = \langle P_{1,2}(\vec{u}(0)\vec{u}(t)) \rangle$ of the unit vector, $\vec{u}$, along the principal rotational axes of the molecule were also obtained. The axes x and z are parallel to C–C and S–O axes, respectively. Once these correlation functions are evaluated and integrated up to infinite time, then the reorientation correlation times τ_1, τ_2 can be obtained. In the present study, the reorientation functions have been evaluated up to 6 ps then were fitted according to the following equation:

$$f(t) = a_1 \, e^{[(b_1 t) + c_1]} + a_1 \, e^{[(b_2 t) + c_2]} \quad (3)$$

Another property computed in this work is the time autocorrelation function of the unit vector along the molecular dipole, $C_\mu(t) = \langle \hat{\mu}(t) \, \hat{\mu}(0) \rangle$, and the corresponding single-molecule dipole reorientation time, τ_μ. These correlation times are experimentally accessible by spectroscopic techniques such as Rayleigh, NMR and time-domain reflectometry. For this reason, the correlation times calculated are discussed and then compared with the corresponding experimental values in Section 3.

3. Results and comparison with previous models

3.1. Thermodynamic properties

Table 2 shows the temperature (T), pressure (P), potential energy (U_{pot}), and molar volume (V_m) calculated using various potential models together with available experimental data. The comparison between calculated results and accurate experimental measurements reveal weaknesses and strengths of the model employed. Note that the system potential energy cannot be determined experimentally but can be compared with the experimentally obtained value of the heat of vaporization via the following equation [42]:

$$\Delta H_{vap}(T) = -U_{pot}(T) + P \, \Delta V + Q_{int} + Q_{ext} \quad (4)$$

where ΔV is the difference between the molar volumes in the gas and liquid phase, and Q_{int} and Q_{ext} correspond to quantum cor-

Table 2
Properties of liquid DMSO calculated from simulations using various rigid models

	RS	P1	P2	VG	Bordat	OPLS	NPS	GOVG	JM4	JM9	Exp
Nominal temperature = 298 K											
T (K)	298.0	298.0	295.7	298.3	296.4	300.8	298.6	298.15	301.5	300.8	298.0
V_m (cm^3)	71.31	71.31	71.31	71.05	71.31	–	71.31	71.31	71.31	71.31	71.31
P (MPa)	8 ± 21 [6]	34 ± 19 [6]	−7 ± 26 [6], −22.85 ± 14.33	8.429 ± 15.62	−19.23 ± 15.24	−50.76 ± 15.50	−17.80 ± 14.34	–	10.00 ± 15.25	−12.92 ± 25.91	0.1013
$-U_{POT}$ (kJ/mol)	36.5	53.9	48.36	52.61	50.78	48.00	49.65	50.41[e]	50.47	50.31	50.45 [55]
	36.22 ± 0.26[a]	53.96 ± 0.22[a]	49.00 ± 0.29[a]	50.401[b]	49.94 ± 0.05[c]	49.90[d]	49.50[d]				
	36.5[g]	52.4[g]	48.85[d]/49.0[g]	53.3[g]	51.30[e]/50.92[e]	47.57[e]/54.07[e]	26.79[e]/26.45[e]				
			48.10[e]/47.57[e]		49.2[g]						
$-U_{EL}$ (kJ/mol)	–	–	19.00	19.88	18.60	16.94	18.15	–	17.48	23.45	–
$\langle F^2 \rangle$ ($\times 10^{-19}$ N^2)	–	–	2.62	3.06	2.90	2.59	2.72	–	2.91	3.32	–
$\langle T^2 \rangle$ ($\times 10^{-21}$ N^2 nm^2)	–	–	4.06	5.08	4.81	3.56	3.95	–	4.29	4.44	–
Nominal temperature = 323 K											
T (K)	–	–	320.4	324.8	323.1	325.2	323.8 ± 15	–	327.3	326.5 ± 8	–
P (MPa)	–	–	−23.96 ± 14.61	4.777 ± 16.56	−14.03 ± 16.51	−42.88 ± 15.66	−18.64 ± 15.63	–	9.759 ± 16.77	−12.83 ± 25.56	0.1013
$-U_{POT}$ (kJ/mol)	–	–	46.97	51.08	49.21	46.57	48.21	–	48.98	48.53	48.75 [57]
$-U_{EL}$ (kJ/mol)	–	–	18.49	19.36	18.07	16.44	17.67	–	17.02	22.75	–
$\langle F^2 \rangle$ ($\times 10^{-19}$ N^2)	–	–	2.74	3.22	3.07	2.73	2.86	–	3.06	3.48	–
$\langle T^2 \rangle$ ($\times 10^{-21}$ N^2 nm^2)	–	–	4.25	5.33	5.08	3.75	4.14	–	4.50	6.09	–
Nominal temperature = 353 K											
T (K)	–	–	352.8	355.7	340.7	355.1	347.2	–	353.5	351.0	–
P (MPa)	–	–	−2.595 ± 16.11	12.76 ± 17.28	−24.656 ± 16.971	−33.805	−22.229 ± 16.117	–	6.552 ± 15.810	−9.925 ± 25.674	0.1013
$-U_{POT}$ (kJ/mol)	–	–	45.29	49.43	47.93	45.05	46.81	–	47.48	46.97	46.89 [57]
$-U_{EL}$ (kJ/mol)	–	–	17.90	18.79	17.68	15.99	17.20	–	16.52	22.09	–
$\langle F^2 \rangle$ ($\times 10^{-19}$ N^2)	–	–	3.02	3.45	3.11	2.91	2.96	–	3.20	3.65	–
$\langle T^2 \rangle$ ($\times 10^{-21}$ N^2 nm^2)	–	–	4.66	5.69	5.15	3.97	4.28	–	4.72	6.32	–
Ensemble[f]	NVT	NVT	NVT	NVT, NPT	NVT, NPT	NPT	NPT	NVT, NPT	NVE	NVE	–

Values are from this work unless specified different.

[a] Ref. [36].

[b] Ref. [35] using NPT, NVT ensemble at T = 298 K and P = 0.1013 MPa.

[c] Ref. [38] at conditions identical with Ref. [35].

[d] Ref. [41] at T = 303 K and P = 0.1013 MPa using NPT ensemble.

[e] Ref. [42] using NPT ensemble: wherever more than one values are present, the first value was obtained using GROMOS standard procedures to derive intermolecular potential parameters for unlike atom pairs and the second value is obtained using the common Lorentz–Berthelot combination rules.

[f] Used by the authors that constructed initially each model.

[g] Ref. [56].

rections for the rigid treatment of the molecule and the classical description of its vibrational energy. Geerke et al. [42] have shown that the sum of the last two terms in Eq. (4) is of the order of −0.01 kJ/mol and $P\Delta V$ is approximately equal to RT = 2.479 kJ/mol.

Table 2 shows that at T = 298 K, the RS model underestimates the experimental value of the heat of vaporization (52.9 ± 0.4 kJ/mol) [55] by about 14 kJ/mol, and the P1 and VG models overestimate the potential energy by about 3 kJ/mol and 2 kJ/mol, respectively. The OPLS and P2 models seem to perform better in reproducing this thermodynamical property, giving 49.2 kJ/mol and 49.0 kJ/mol, respectively. Our results are in good agreement with those presented by Skaf in a previous study where he employed these models with 864 molecules in the central simulation box [56]. For the pressure, although the RS, VG, JM4, and JM9 do not reproduce satisfactorily the experimental value of 1 bar [55], they do perform better than the remaining models. At T = 323 K, the VG, JM4, and JM9 perform better than the remaining in reproducing the pressure, and the Bordat, NPS, JM4, and JM9 perform well with respect to the experimental value of the enthalpy of vaporization [57]. Finally at T = 353 K, the P2, VG, JM4 and JM9 perform better than the remaining models in reproducing the pressure and the Bordat, NPS, JM4 and JM9 are better in reproducing the experimental value of the enthalpy of vaporization [57].

3.2. Microscopic structure

MD simulations can provide a clear picture about the local structure in molecular system via the calculation of the site–site pair distribution functions [32]. The atom–atom distribution functions obtained appear to be, to some extent, insensitive to the potential model employed. Thus, it seems that the hard core packing determines the microscopic structure and therefore subtle differences in describing weak bonds cannot alter significantly the overall picture [6,41]. However, the differences can be enhanced when we calculate the weighted sum of the heavy O, S, and C atom–atom pair distributions. This weighted sum is presented in Fig. 2 along with the experimental results obtained by Luzar et al. at 298 K [6]. It should be noted that the P1 model has the poorest agreement with the experiment and the RS model performs better than all the rest on reproducing the weighted sum. Neglecting the P1 model, almost all the models shown in Fig. 2 are in satisfactorily agreement with each other at intermolecular distances around the second peak (0.6–0.7 nm). However, none of the models can reproduce satisfactorily the experimental results at shorter distances (<0.5 nm) and especially the plateau observed between 0.4 nm and 0.45 nm. This will be discussed further in Section 4.

As shown in Fig. 3, the weighted sum of pair distribution functions of the heavy atoms for both the DMSO-*d*0 and DMSO-*d*6 molecules do not depend on the temperature, for the temperature range studied here (298–353 K). By integrating these distribution functions up to first minimum, which is around 0.71 nm, the number of neighbour atoms in the first shell is found to be around 12 in all cases, a typical number for the liquid phase. Torii and Tasumi had already shown [58] that the molecules are arranged side by side and oriented in an anti-parallel manner in the 0.3–0.4 nm region and arranged head-to-tail in the 0.4–0.6 nm region.

3.3. Diffusion coefficients

The values of the DMSO-*d*0 and DMSO-*d*6 self-diffusion coefficients obtained from the present MD study are presented and compared with previous models and available experimental results in Table 3. Our results on DMSO-*d*0 diffusivity using the JM4 and JM9 models agree with the various available experimental measurements at low and high temperatures (see Fig. 4), but overestimate the diffusion coefficient for temperatures between 310 K and 325 K. Given that the values from the current work are the lowest values among all the available theoretical calculations, this disagreement may reveal either some interesting dynamical phenomena at these particular temperatures that cannot be described with the usual assumptions in classical, rigid MD calculations [59]

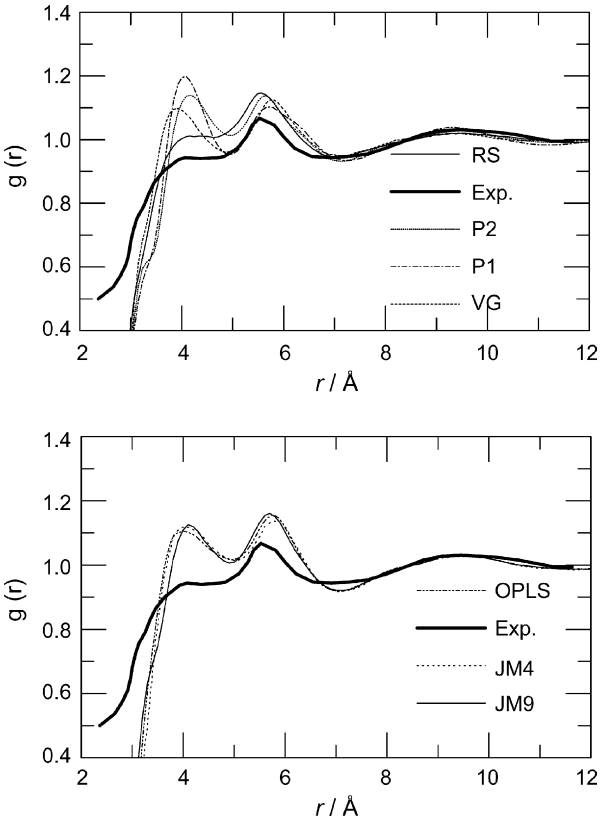

Fig. 2. Comparison between the calculated and the experimental weighted sum of the heavy atom–heavy atom pair distribution function of liquid DMSO at T = 298 K and P = 1 bar. See text for details. The data points for the previous models were provided by Skaf.

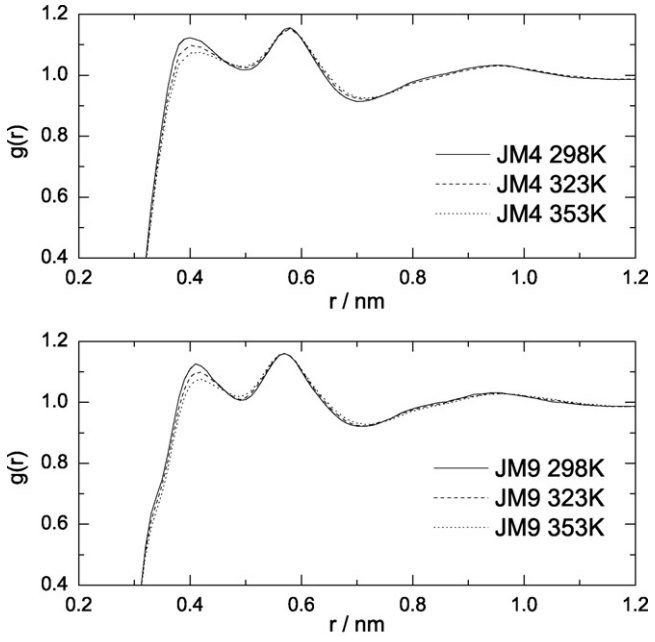

Fig. 3. Temperature dependence of the heavy atom–heavy atom pair distribution function of liquid DMSO using the JM4 and JM9 models.

Table 3
Temperature dependence of self-diffusion coefficients (in 10^{-9} m^2 s^{-1}) calculated from simulations that employed rigid models of the DMSO molecule, and compared with experimental values

T (K)	Simulations/Experimental	D	T (K)	Simulations/Experimental	D	T (K)	Simulations/Experimental	D
288.15	Experimental	0.57 [27]	300.8	OPLS	1.212[d]	327.3	JM4	1.303[d]
288.2	Experimental	0.6505[b]	300.8	JM9	0.6901[d]	328.1	Experimental	1.266 [28]
295.7	P2	1.194[d]	301.5	JM4	0.7990[d]	339.3	JM4	1.5096[d]
296.4	Bordat	0.9632[d]	303	NPS	0.89 [41]	340.7	Bordat	1.675[d]
297.5	Bordat	0.88 ± 0.02 [41]	303	OPLS	0.95 [41]	347.2	NPS	1.879[d]
297.5	JM4	0.7310[d]	303	P2	1.15 [41]	348	Senapati[a]	1.988
298	RS	2.5 [56]	306.1	JM4	0.9560[d]	350.4	JM4	1.8926[d]
298	P1	0.8 [56]	308.1	Experimental	0.890 [28]	351.0	JM9	1.528[d]
298	P2	1.2 [56]	308.1	Experimental	0.91 [27]	352.8	P2	2.396[d]
298	VG	1.1 [41]	308.2	Experimental	1.073[b]	353.5	JM4	1.793
298	VG	1.3 [41]	310.3	JM4	1.1900[d]	355.1	OPLS	2.190[d]
298	OPLS	0.9 [56]	318.1	Experimental	1.067 [28]	355.7	VG	1.609[d]
298	Senapati[a]	1.048	320.3	P2	1.601[d]	373	Senapati[a]	2.452
298	GOVG	1.1 [42]	322.5	JM4	1.3402[d]	354.6	JM4-*d*6	1.7249[d]
298.1	Experimental	0.73 [27]	323	Senapati[a]	1.679	288.15	Experimental-*d*6	0.51 [27]
298.1	Experimental	0.731 [28]	323.1	Bordat	1.304[d]	296.8	JM4-*d*6	0.7246[d]
298.15	Experimental	0.768[c]	323.8	NPS	1.432[d]	298.15	Experimental-*d*6	0.65 [27]
298.3	VG	0.8589[d]	324.8	VG	1.227[d]	307.5	JM4-*d*6	0.8923[d]
298.6	NPS	1.082[d]	325.2	OPLS	1.737[d]	308.15	Experimental-*d*6	0.82 [27]
299.2	Experimental	0.8331[b]	326.5	JM9	1.125[d]	328.2	JM4-d6	1.2640[d]

Results for the fully deuterated isotope are denoted with -*d*6.
[a] Read off from Fig. 3 in Ref. [46] where a fully flexible non-polarizable model was employed.
[b] Read off from Fig. 3 in Ref. [23].
[c] Read off from Fig. 1 in Ref. [26].
[d] From this work.

or possibly some problems with the experimental measurements. As one could have expected the value of the self-diffusion coefficient is smaller in the DMSO-*d*6 case, shown in Table 3, reflecting an increase in the molecular weight for the fully deuterated molecule. This difference becomes smaller with increasing temperature.

Table 3 shows that the RS model overestimates the value of the self-diffusion coefficient by a factor of 3.4, while the P1 model yields results very close to the available experimental values. Results from the current work employing the P2 model are in slight variance with results obtained by Liu et al. who employed the same potential model. The present study using the P2 model and an NVE statistical ensemble yields a value of 1.15 × 10^{-9} m^2 s^{-1}, very similar to the value of 1.2 × 10^{-9} m^2 s^{-1} reported by Skaf [56] for this model. Liu et al. [35] reported a much higher value (1.7 × 10^{-9} m^2 s^{-1}) using the same model but employing an NPT ensemble. In order to investigate the ensemble and simulation time dependence of the diffusion coefficient values of DMSO-*d*0, we have performed a much longer duration simulation for the P2 model using the NPT ensemble and 864 molecules in the simulation box. Only negligible differences were observed between the results obtained using the NVE and NPT ensembles under these conditions. Therefore, the higher D values presented by Liu et al. [35] might reflect some difficulties caused by statistical uncertainties because in that work the phase space trajectory had a length of only 60 ps. As Senapati [46] pointed out another possible source of error in the study by Liu et al. [35] might be their neglect of the interactions which occur beyond their cut-off distance. Table 3 shows that the theoretical predictions of all the models, excluding the RS, are very close to each other. The models presented in this work performed slightly better than the VG and OPLS models.

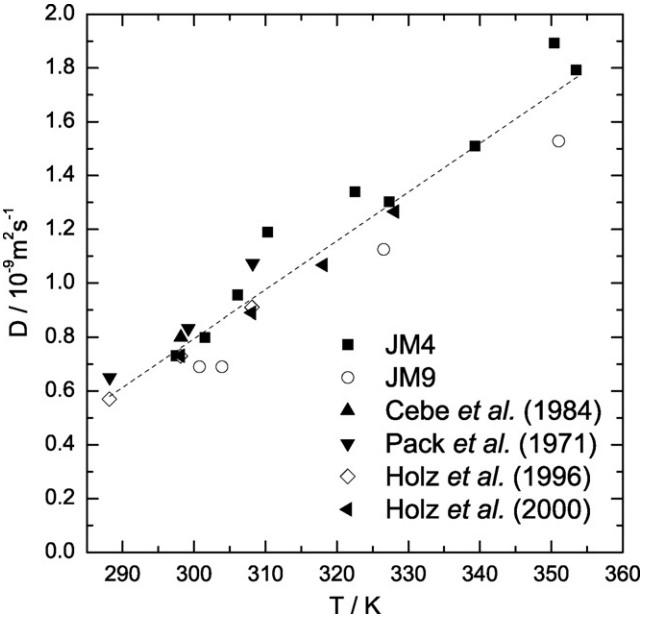

Fig. 4. Dependence of the DMSO-*d*0 translational self-diffusion coefficient on temperature at P = 1 atm. Experimental results are also presented for comparison. The data are fitted by a straight line D (10^{-9} m^2 s^{-1}) = −4.644 + 0.01813 T (K).

Various theoretical models are available to reproduce the diffusion coefficient values in the gas phase [54]. In liquids, however, simple empirical equations are often used to describe the temperature and density dependence of diffusion coefficients. A simple parabolic function, $D = A + BT + CT^2$ is commonly employed [60] to describe the diffusivity at constant density. In the present work, even a simple linear function seems adequate over the temperature range 298–353 K, as shown in Fig. 4. Taking together all the available experimental data and the results from our JM4 and JM9 models, we get D (10^{-9} m^2 s^{-1}) = −4.644 + 0.01813 T (K). A similar analysis gives for the DMSO-*d*6 case: D (10^{-9} m^2 s^{-1}) = −4.775 + 0.01834 T (K). In order for a particle to move in a diffusion process, a characteristic free volume is needed and thus an amount of activation energy, which corresponds to the work required to create such a volume, is required. An equation that is usually employed [4] is of a simple exponential type $D = C\exp(-E_\alpha/k_B T)$ or in logarithmic form, $\log D = A - B\,1000\,T^{-1}$, where B corresponds to activation energy, E_α. Taking into account results from this study the activation energy was found equal to 13.99 kJ/mol (see Fig. 5), which compares satisfactorily with the values of 11.65 kJ/mol and 14.70 kJ/mol found for *N*,*N*-DMF [61] and acetone [27], for the range of tem-

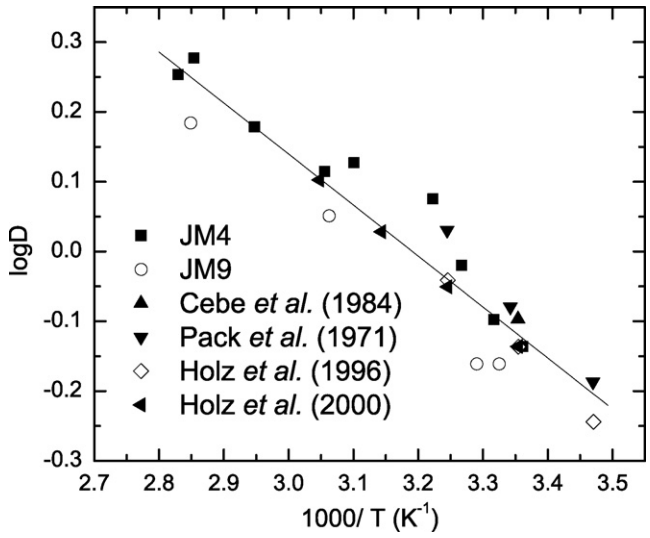

Fig. 5. Semi-logarithmic plot of the simulated and experimental liquid DMSO self-diffusion coefficient dependence on the reciprocal temperature.

peratures 222–373 K and 288–308 K, respectively. Using a similar procedure in the fully deuterated case, one gets an activation energy of 15.22 kJ/mol, which is around 9% higher than in the lighter DMSO-*d*0.

3.4. Shear viscosity

Numerous studies on the influence of temperature on the viscosity of pure fluids have been carried out [4]. The shear viscosity of gases increases with temperatures below the critical point. However, it increases with the inverse of temperature for $T > T_c$, and for higher values of pressure. For liquids a decrease with temperature is observed [4]. Various equations, such as $\ln \eta = A + B/T$ or $\ln \eta = A_1 + B_1/(T + C_1)$ (de Guzman–Andrade equation), $\eta = A_2 \exp[B_2/(T - T_0)]$ (Vogel–Fulcher–Tamman–Hesse equation, VFTH) or $\eta = A_3[T/T_3 - 1]^{-m}$ (a power-law form) are commonly employed [4,62,63] for temperatures lower than the normal boiling point. In the relation proposed by de Guzman and Andrade, $B = E_\eta/R$, where E_η is the energy of viscous flow and A is usually considered to be a constant, although Eyring suggested that is a temperature-dependent quantity [4].

Bicknell et al. [25] used a capillary tube viscometer to measure the viscosity of pure DMSO over a wide temperature range

Table 4
Temperature dependence for values of the shear viscosity, η (in cP = 10^{-2} Pa s), calculated from simulations that employed rigid models of the DMSO molecule, and compared with experimental results

T (K)	η (cP) DMSO-*d*0	T (K)	η (cP) DMSO-*d*0	T (K)	η (cP) DMSO-*d*6
293	2.2159[a], 2.473[b], 2.198[c]	317	1.4153[a]	298	2.180[d], 2.195[e], 2.198[f]
295	2.1229[a], 2.12[g]	318	1.41[g], 1.394[h], 1.380[d]	298	2.300[i]
297	2.0374[a]	319	1.3704[a]	308	1.800[d]
298	2.00[g], 2.003[h], 1.989[j]	321	1.3280[a]	318	1.510[d]
298	1.991[k], 1.9848[l], 1.74 ± 0.14[m]	323	1.2880[a], 1.372[b], 1.294[n]		
298	1.22[o], 1.26 ± 0.24[p], 1.29 ± 0.27[q]	323	1.168[i], 0.9593[r], 0.6864[s]		
298	1.980[d], 1.28[s], 1.24[t]	323	0.7789[t], 1.0322[u], 1.080[v]		
298	2.090[i], 1.991[n], 1.3023[r]	325	1.2490[a]		
298	0.922[s], 1.258[u], 1.971[v]	327	1.2125[a]		
298	1.980[c], 1.888[w]	329	1.1774[a]		
299	1.9571[a]	331	1.1443[a]		
301	1.8817[a]	333	1.1126[a], 1.124[b], 1.12[g]		
303	1.8100[a], 2.003[b], 1.794[c]	338	1.038[h]		
305	1.7430[a]	343	0.975[b], 1.00[g]		
307	1.6803[a]	353	0.849[b], 1.110[n], 0.8154[i]		
308	1.639[d], 1.636[c]	353	0.7809[r], 0.5314[s], 0.5836[t]		
309	1.6210[a], 1.65[g]	353	0.7742[u], 0.8345[v]		
311	1.5652[a]	363	0.740[b]		
313	1.5126[a], 1.640[b]	373	0.680[b]		
315	1.4626[a]	403	0.570[b]		

[a] Measured in Ref. [25].
[b] Measured in Ref. [21].
[c] Measured in Ref. [64].
[d] Measured in Ref. [27].
[e] Measured in Ref. [66].
[f] Measured in Ref. [89].
[g] Measured in Ref. [24].
[h] Measured in Ref. [22].
[i] Calculated in this work using the JM4 model.
[j] Measured in Ref. [88].
[k] Measured in Ref. [2] as mentioned in Ref. [88].
[l] Measured in Ref. [65] as mentioned in Ref. [88].
[m] Calculated using non-equilibrium molecular dynamics in Ref. [38].
[n] Calculated in this work using the JM9 model.
[o] Calculated in Ref. [42].
[p] Calculated in Ref. [35] using the Einstein relation.
[q] Calculated in Ref. [35] using the Green–Kubo relation.
[r] Calculated in this work using the NPS model.
[s] Calculated in this work using the OPLS model.
[t] Calculated in this work using the P2 model.
[u] Calculated in this work using the VG model.
[v] Calculated in this work using the Bordat model.
[w] Read off from Ref. [26].

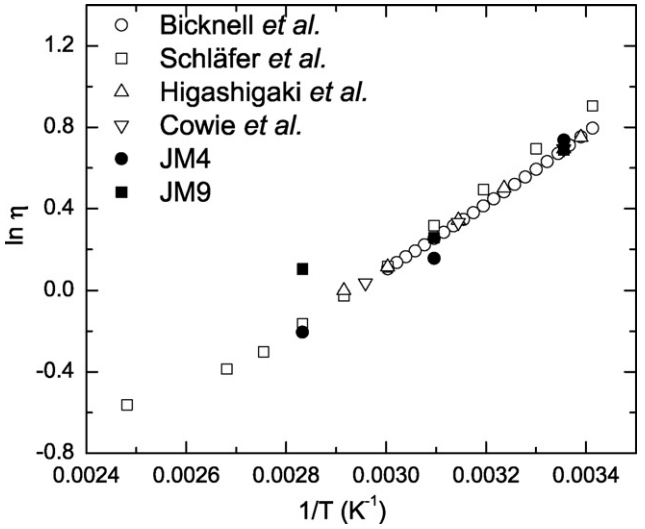

Fig. 6. Calculated and experimental temperature dependence of DMSO-*d*0 shear viscosity. Measurements by Bicknell et al. [25] (open circles), Schläfer and Schaffernicht [21] (open squares), Higashigaki et al. [24] (open up triangles) and Cowie and Toporowski [22] (open down triangles) are compared with calculated results using the JM4 (filled circle) and JM9 (filled squares) models.

of 293–323 K. The values of the DMSO-*d*0 and DMSO-*d*6 shear viscosities obtained from the present MD study are presented and compared with previous models and available experimental results in Table 4 at various temperatures. It should be mentioned that all the previous models (P2, OPLS, GOVG, NPS, Bordat, VG) significantly underestimate the shear viscosity values. As shown in Fig. 6, the results for the DMSO-*d*0 viscosity using the JM4 model, are in good agreement with experimental measurements [25].

Bicknell et al. mentioned that while the equation $\ln \eta = A + B/T$ is sufficient for many non- or weakly associated fluids but for strongly associated solvents, such as water, an extension of de Guzman–Andrade's equation ($\ln \eta + 1/3 \ln V_m = \ln A' + c/V_m T$), where V_m is the specific volume of the liquid, is usually required to describe the curved plots (see Fig. 6). This behavior was observed for the DMSO molecule, especially for the values obtained at higher temperatures by Schläfer and Schaffernicht [21]. Bicknell et al. described the temperature dependence of shear viscosity using smooth, curved plots, excluding the possibility that the association structure of DMSO breaks down over the temperature range studied. Indeed, when we fitted the results to an extension of de Guzman–Andrade's equation [4], a graph less curved at high T than from the original de Guzman–Andrade equation was obtained. Bicknell et al. obtained a value of c equal to 1182 $cm^3\,K\,g^{-1}$, which is similar in magnitude to the values of c obtained here, 1102.5 $cm^3\,K\,g^{-1}$, where we included in the data sets the experimental measurements from Refs. [2,21,22,24,25,27,64,65] and theoretical results using the JM4 and JM9 models.

Unfortunately there are not many measurements for the DMSO-*d*6 shear viscosity. Sacco and Matteoli [66], and Holz et al. [28] obtained 2.195 cP, and 2.198 cP, respectively, at 298 K. Holz et al. obtained values of 2.180 cP, 1.800 cP, and 1.510 cP for the DMSO-*d*6 at temperatures 298 K, 308 K, and 318 K, respectively [27]. In order to examine the isotopic dependence of shear viscosity, the simple equation, $\ln \eta = A + B/T$ was used. By fitting this equation to results shown in Fig. 6 for DMSO-*d*0, the activation energy was found to be 13.07 kJ/mol. Taking into account all the available experimental results, a value of 15.26 kJ/mol was observed for the DMSO-*d*6 case. Note that when we took into account only the results obtained by Holz et al. [27], a value of 13.88 kJ/mol was obtained which is closer to the DMSO-*d*0 case. Holz et al. [27] have investigated the dynamic isotope effect in a number of liquids and examined the ratios $D_1/D_2 = \eta_2/\eta_1$, where the subscripts 1 and 2 refer to protonated and deuterated species, respectively. These authors suggested that when this ratio has a value closer to $(I_2/I_1)^{1/2} = I_r^{1/2}$, where I is the moment of inertia, than to $(m_2/m_1)^{1/2} = m_r^{1/2}$, a strong coupling between translation and rotation then exists. In the case of DMSO, $m_r^{1/2}$ is equal to 1.038, and $I_{r,a}^{1/2}$, $I_{r,b}^{1/2}$, $I_{r,c}^{1/2}$ take values of 1.080, 1.130 and 1.100, where $I_{r,i}$ denotes the I_r ratio for the i-axis. The values of $\eta_r = \eta_2/\eta_1$ are 1.101, 1.098 and 1.094 at temperatures of 298 K, 308 K and 318 K, respectively and the values of D_1/D_2 are 1.12, 1.12 and 1.11 at temperatures of 298 K, 308 K and 318 K [27]. While it is fair to say that the values of $m_r^{1/2}$ and $I_r^{1/2}$ do not differ much, it is clear that the values of $D_1/D_2 = \eta_2/\eta_1$ are closer to $I_r^{1/2}$. This suggests that there is a significant translation–rotation coupling which shows no temperature dependence for the range of 298–318 K.

3.5. Rotational dynamics

Infra-red absorption, Raman band profiles, Rayleigh light scattering, NMR spin–lattice relaxation times, and time-resolved fluorescence depolarization measurements are among some of the methods used to study orientation processes [32]. In order to describe in a quantitative way the molecular reorientation processes one needs to obtain the reorientation correlation functions, $C_{1,2}(t) = \langle P_{1,2}(\vec{u}(0)\vec{u}(t))\rangle$. These functions can act as a measure of the average rate at which the molecules in an interacting sample lose "memory" of their original orientation. Information pertinent to $\langle P_1\rangle$ can be provided by Infra-red spectra, and information pertinent to $\langle P_2\rangle$ can be extracted from Raman, Rayleigh and NMR experiments. Raman experiments, in principle, contain much more information about molecular rotation than the corresponding spin experiments, because the time dependence of this correlation function is obtained, rather than just its time integral. It should be noted at the outset of our discussion that Infra-red, Raman and NMR experiments determine the single molecule relaxation rates, while depolarized Rayleigh light scattering probes both the single particle and the pair correlated reorientation process. Therefore, in principle, the Rayleigh relaxation times are expected to be higher than the corresponding NMR times.

In this work, the following notation for the rotational axes and the respective moment of inertia was used: I_A (for rotation along x-axis, which is parallel to C–C axis), I_B (for rotation along z-axis, which is parallel to S–O bond), and I_C (for rotation along the y-axis, which is perpendicular to the previous two axes). Strictly speaking DMSO molecules are of C_S symmetry. Forel et al. using Infra-red and Raman spectra, obtained the following values of the DMSO-*d*0 moments of inertia: $I_A = 71.84$, $I_B = 73.15$, $I_C = 119.83$ g Å^2 mole^{-1} [67]. Thus, in the analysis of the results, the DMSO molecule can be treated as an oblate symmetric top to simplify the study on the rotational motion, because $I_A \approx I_B$. In order to describe the rotation dynamics, the autocorrelation functions of both the angular velocities and torques have been calculated. All the autocorrelation functions of the angular velocities show a (negative) minimum at around 0.2 ps. The corresponding functions for the torques also show a minimum, again with a negative value, at around the same time and then show a local maximum, with a positive value around 0.3 ps. A second minimum with a negative value at around 0.4 ps is observed, which implies the existence of a cage effect (see discussion below). At 298 K, the root-mean-squared (RMS) value of the torque per molecule is 6.50×10^{-20} J and 6.46×10^{-20} J for the DMSO-*d*0 and DMSO-*d*6 molecules. These values result in reorientation correlation times (averaged over the *a*- and *b*-axes) of 2.9 ps and 3.0 ps, respectively. Our results compare quite well with values by Clark and co-workers for liquid CS_2, where theirs simulation gave a reorientation correlation time of 1.5 ps at 300 K, and

Table 5
Theoretical values of rotational relaxation times (τ_1) at various temperatures

T (K)	τ_1 (ps)
298	10.58[a]
298	8.71[b]
298	10.18[c]
298	8.43[d]
303	6.16[e]
303	6.67[f]
303	6.91[g]
297.5	8.850[h], 5.60[i]
298	4.83[j], 7.46[k]
298	6.31[l], 9.72[m]
310.3	6.35[h], 4.53[i]
322.5	6.20[h], 3.60[i]
323	3.64[j], 5.73[k]
323	4.69[l], 7.00[m]
339.3	4.58[h], 3.10[i]
350.4	4.30[h], 2.85[i]
353	2.95[j], 4.51[k]
353	3.76[l], 5.64[m]
296.8	9.15[n], 5.90[o]
307.5	7.45[n], 4.81[o]
328.2	7.20[n], 4.10[o]
354.6	4.80[n], 3.15[o]

[a] Obtained in Ref. [38] for the S–O bond vector using the Bordat model and employing a stretched exponential, $\exp(-t/\alpha)^{\beta}$, exponential function.
[b] As in footnote a but for the S–CH_3 bond.
[c] Obtained in Ref. [38] for the S–O bond vector using the Bordat model and employing an exponential (Debye model) fitting function.
[d] As in footnote c but for the S–CH_3 vector.
[e] Calculated in Ref. [41] using the P2 model.
[f] Calculated in Ref. [41] using the OPLS model.
[g] Calculated in Ref. [41] using the NPS model.
[h] For the *a* axis of the DMSO-*d*0 using the JM4 model.
[i] For the *b* axis of the DMSO-*d*0 using the JM4 model.
[j] From this work for the *a* axis using the NPS model.
[k] From this work for the *b* axis using the NPS model.
[l] From this work for the *a* axis using the Bordat model.
[m] From this work for the *b* axis using the Bordat model.
[n] For the *a* axis of the DMSO-*d*6 using the JM4 model.
[o] For the *b* axis of the DMSO-*d*6 using the JM4 model.

theirs torque RMS values were equal to 1.4×10^{-20} J and 1.5×10^{-20} J using high-resolution spontaneous Raman, and simulation, respectively.

The short-time behavior of the $C_2(t)$ correlation function can be written as $1-(3kT/I)t^2+[4(kT/I)^2+(8I^2)^{-1}\langle T^2\rangle]t^4+O(t^6)$. Thus, the initial curvature (second moments) of these correlation functions depend only on the temperature and the moment of inertia, but not on the intermolecular forces. For an initial period of around 0.1 ps, the $C_2(t)$ correlation function shows a decay which is almost indistinguishable from those of the free rotational motion, because intermolecular torques have not yet built up to have an effective power on the motion. Thus, the first part of the reorientation functions can be described by the simplest inertial model; the free rotor which is accurate for gaseous systems but not for liquids. This model is valid only at very short times in our case, because during that short period of time there are very few collisions and therefore the rotational motion is not strongly affected by intermolecular forces. In the time interval between 0.1 and ~0.4 ps, the intermolecular forces produce significant hindering of the rotation, and so the reorientation takes place more slowly than in the free rotational motion. At times higher than ~0.6 ps, the rotational motion has experienced the intermolecular torques, and the average correlation is indistinguishable from that of random, exponential decay. Usually the $C_2(t)$ reorientation functions decay quicker than the corresponding $C_1(t)$ functions, but this is a direct effect of the definitions of the Legendre polynomials.

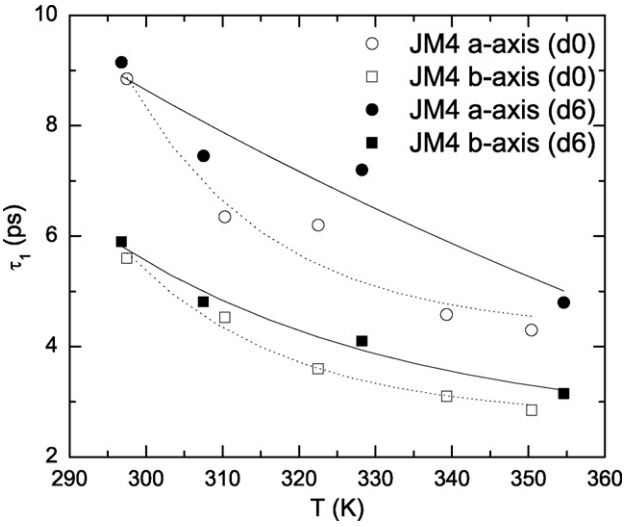

Fig. 7. DMSO-*d*0 and DMSO-*d*6 rotational correlation times (τ_1) and exponential fits to the data as a function of temperature.

Neither $C_1(t)$ nor $C_2(t)$ could be fitted by a single exponential. This is in contrast to predictions based on stochastic models, which assume that the reorientation occurs as a series of thermally activated jumps over a potential energy barrier. These models guesstimate exponentially decaying reorientation correlation functions which are never observed experimentally. In order to make a quantitative analysis of the rotational dynamics we evaluated the reorientation correlation times, $\tau_{l,a}$, for all the analyzed molecular directions as the time integrals: $\tau_{l,a}=\int_0^{\infty} C_{l,a}(t)\,dt$ using a bi-exponential function, $a_1\exp(b_1\,t+c_1)+a_2\exp(b_2\,t+c_2)$, and the correlation times are presented in Tables 5 and 6. In all temperatures studied, the $\tau_{1,a}$ and $\tau_{2,a}$ values are greater than the corresponding $\tau_{1,b}$ and $\tau_{2,b}$ values, respectively [68]. This behavior also becomes obvious from the time evaluation of the correlation functions. Such a feature can be easily explained in terms of the moments of inertia which correspond to the *a* and *b* principal axes of the molecule [69]. Tables 5 and 6 and Figs. 7 and 8 show that the relaxation times decrease systematically with increasing temperature. Unfortunately, there are not any experimental measurements on τ_1 for DMSO and therefore only a comparison between different theoretical models can be made at this time.

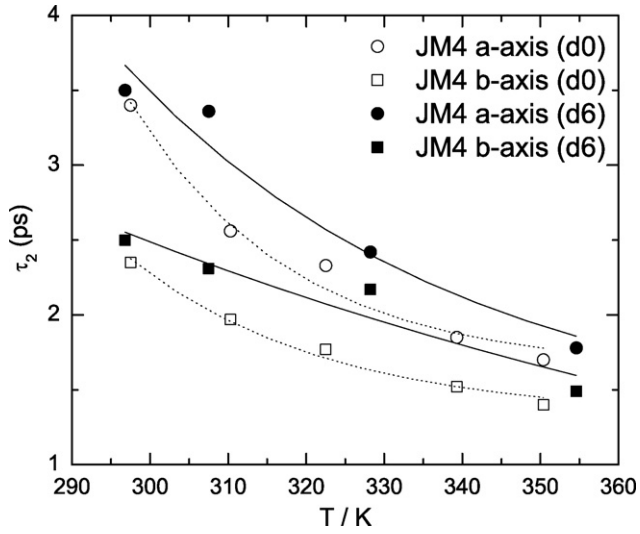

Fig. 8. Rotational correlation times (τ_2) of DMSO-*d*0 and DMSO-*d*6 molecules as a function of temperature.

Table 6
Experimental and theoretical values of rotational relaxation times (τ_2) at various temperatures

T (K)	τ_2 (ps)
295	4.4[a], 17.7[b]
296.8	3.5[c], 2.5[d]
297.5	3.4[e], 2.35[f]
298	1.71[g], 2.39[h]
298	2.25[i], 3.15[j]
298	3.50[k], 3.14[l]
298	3.21[m], 2.89[n]
298	1.8[o], 3.2[p]
298	3.3[q], 6.6[r]
298	4.9[s], 3.9[t]
303	3.2[u], 3.0[v]
303	3.2[w], 3.7[x]
303	5.2[y]
307.5	3.36[c], 2.31[d]
310.3	2.56[e], 1.97[f]
317	3.0[x], 4.0[y]
322.5	2.33[e], 1.77[f]
323	1.30[g], 1.82[h]
323	1.63[i], 2.26[j]
323	3.6[z]
328.2	2.42[c], 2.17[d]
332	2.4[x], 3.2[y]
333	1.9[a], 8.8[b]
333.15	4.2[ω]
339.3	1.85[e], 1.52[f]
343.15	3.4[ω]
346	2.0[x], 2.6[y]
350.4	1.70[e], 1.40[f]
353	1.03[g], 1.43[h]
353	1.31[i], 1.83[j]
353	1.8[z]
354.6	1.78[c], 1.49[d]

[a] Measured in Ref. [70] for DMSO-*d*6 for 265 cm^{-1} vibrational transition.
[b] Measured in Ref. [70] for DMSO-*d*6 for 2248 cm^{-1} vibrational transition.
[c] For the *a* axis of the DMSO-*d*6 using the JM4 model.
[d] For the *b* axis of the DMSO-*d*6 using the JM4 model.
[e] For the *a* axis of DMSO-*d*0 using the JM4 model.
[f] For the *b* axis of DMSO-*d*0 using the JM4 model.
[g] For the *a* axis of DMSO-*d*0 using the NPS model.
[h] For the *b* axis of DMSO-*d*0 using the NPS model.
[i] For the *a* axis of DMSO-*d*0 using the Bordat model.
[j] For the *b* axis of DMSO-*d*0 using the Bordat model.
[k] Obtained in Ref. [38] for the S–O bond vector using the Bordat model and employing a stretched exponential, $\exp(-t/\alpha)^{\beta}$, exponential function.
[l] As in footnote k but for the S–CH_3 bond.
[m] Obtained in Ref. [38] for the S–O bond vector using the Bordat model and employing an exponential (Debye model) fitting function.
[n] As in m but for the S–CH_3 vector.
[o] Calculated in Ref. [35] using the RS model.
[p] Calculated in Ref. [35] using the P2 model.
[q] Calculated in Ref. [75] using the flexible model by Fox et al. [43].
[r] Calculated in Ref. [75] using the rigid model by Fox et al. [43].
[s] Calculated in Ref. [42] using the GOVG model.
[t] From Ref. [35] using the VG model.
[u] Calculated in Ref. [41] using the P2 model.
[v] Calculated in Ref. [41] using the PLS model.
[w] Calculated in Ref. [41] using the NPS model.
[x] Measured in Ref. [73] using ^{33}S nuclear spin relaxation rate.
[y] Measured in Ref. [73] using ^{17}O nuclear spin relaxation rate.
[z] Obtained in Ref. [71] by measuring the temperature dependence of various DMSO depolarized Raman linewidths.
[ω] Rayleigh relaxation times taken from Ref. [24].

Vishnyakov et al. showed that at 303 K, the τ_1 values increase in the order NPS > OPLS > P2 (see Table 5). Note that regarding the Bordat model, the values increase in the order SO bond [38] > *b*-axis (this work) > S–CH_3 bond [38] > *a*-axis (this work). Regarding the JM4 model, the values increase in the order: *a*-axis (DMSO-*d*6) > *a*-axis (DMSO-*d*0) > *b*-axis (DMSO-*d*6) > *b*-axis (DMSO-*d*0).

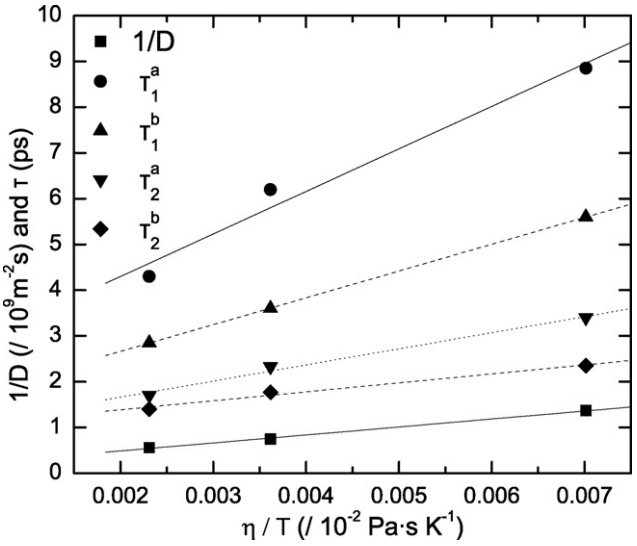

Fig. 9. Stokes–Einstein–Debye plots for liquid DMSO-*d*0 using the JM4 model.

Orientation dynamics in simple liquids can be generally discussed using hydrodynamic theory, which predicts a linear increase with the inverse temperature of the orientation relaxation times in semi-log plots (Frenkel's equation), and a linearly increase of τ_2 with increase of the ratio viscosity/temperature (see Fig. 9). Frenkel's equation [70] can be written as $\tau_2 = \tau_0 \exp(E_{0r}/k_B T)$, where τ_0 is the oscillation period of the molecule in the equilibrium position and E_{0r} is the activation energy for the transition of a molecule between two equilibrium positions. Singurel et al. obtained the average lifetime of molecular reorientation, $\tau_r(T)$, by measuring the temperature dependence of various depolarized Raman linewidths, $\Delta\delta(T)$, for the DMSO-*d*0 and using the equation $\Delta\delta(T) = 1/(\pi c \tau_r(T))$ [71], where c is the velocity of light in vacuum. They found that the Raman linewidth of pure liquids was a linear function of the reciprocal viscosity coefficient, and they obtained $\tau_2 = 3.6$ ps and 1.8 ps at temperatures of 323 K and 353 K, respectively. They then used Frenkel's equation and obtained a value of 7.5 ± 1.3 kJ/mol for the potential barrier of the reorientation. The same authors obtained $E_{0r} = 8.4 \pm 0.84$ kJ/mol, using equation $\eta = C \exp(E_{0r}/k_B T)$ and shear viscosity values from Cowie and Toporowski [22]. As shown in Fig. 8, our results using the JM4 model for the temperature range between 297 K and 350 K show that the orientation dynamics is a thermally activated process which follows an Arrhenius law with an activation energy of 11.1 kJ/mol and 8.36 kJ/mol for the axes *a* and *b* of DMSO-*d*0, and 10.8 kJ/mol and 7.45 kJ/mol for the axes *a* and *b* of DMSO-*d*6 molecules.

If the rotational motion can be described in terms of rotational diffusion, then the Debye–Stokes–Einstein equation predicts that $D_{trans} = k_B T/6\pi\eta r_H = 4r_H^2 D_{rot}/3$. D_{trans} is the translation diffusion coefficient, $D_{rot} = \int_0^{\Delta t} \langle \omega_i(0)\, \omega_i(t) \rangle \, dt$ is the corresponding rotational diffusion, η the shear viscosity and r_H is the effective hydrodynamic radius. Then the relaxation time for an lth order Legendre polynomial is given by $\tau_{l,rot} = 1/(l(l+1)D_{rot})$. For example, for the dielectric signal, $l = 1$, and for the NMR measurements mentioned here, $l = 2$. The ratio between corresponding values of τ_1 and τ_2 reveals the type of the reorientation motion. Thus, for a rotational molecular process with relatively small angular steps, the rotational motion can be treated as diffusional and τ_1/τ_2 approaches 3. On the other hand, when the rotational motion consists of larger angular steps, the τ_1/τ_2 ratio is expected to be smaller than 3 (see also Section 3.7). In the latter type of the reorientation, the time between collisions, τ_{BC}, is small compared to the mean period of rotation of the free rotor [72], $\tau_F = \sqrt{I/k_B T}$, and a molecule can rotate through

Table 7
Ratios of rotational relaxation times, (τ_1/τ_2), at various temperatures

T (K)	$(\tau_1/\tau_2)^a$	$(\tau_1/\tau_2)^b$	T (K)	$(\tau_1/\tau_2)^a$	$(\tau_1/\tau_2)^b$	T (K)	τ_1/τ_2
296.8	2.61[c]	2.36[c]	323	2.87[d]	3.09[d]	298	3.02[e]
297.5	2.61[f]	2.38[f]	328.2	2.98[c]	1.89[c]	298	2.77[g]
298	2.83[h]	3.12[h]	339.3	2.48[f]	2.04[f]	298	3.17[i]
298	2.81[d]	3.08[d]	350.4	2.53[f]	2.03[f]	298	2.92[j]
307.5	2.22[c]	2.08[c]	353	2.87[h]	3.16[h]		
310.3	2.48[f]	2.30[f]	353	2.87[d]	3.08[d]		
322.5	2.66[f]	2.03[f]	354.6	2.70[c]	2.11[c]		
323	2.80[h]	3.14[h]					

[a] For the *a* axis of the DMSO.
[b] For the *b* axis of the DMSO.
[c] Obtained using the JM4 model for DMSO-*d*6.
[d] Obtained using the Bordat model for DMSO-*d*0.
[e] Calculated in Ref. [38] for the S–O bond vector using the Bordat model and employing a stretched exponential, $\exp(-t/\alpha)^{\beta}$, fitting function.
[f] Obtained using the JM4 model for DMSO-*d*0.
[g] As in footnote e but for the S–CH_3 bond.
[h] Obtained using the NPS model for DMSO-*d*0.
[i] Calculated in Ref. [38] for the S–O bond vector using the Bordat model and employing an exponential (Debye model) fitting function.
[j] As in footnote i but for the S–CH_3 vector.

a very small angle before suffering a reorienting collision (small-step diffusion). In the Debye model, where the reorientation is only slightly affected by rotranslational coupling, the molecule can rotate through a very small angle before suffering a reorienting collision. If the ratio of the relaxation times is around 1, then we have jump diffusion with a uniform distribution of angle amplitudes. The chaotic reorientation correlation time, τ_2, can be obtained by Debye's equation [70] $\tau_2 = (4\pi\alpha^3\eta)/(3k_B T)$ where η is the viscosity coefficient and α is the effective molecular radius. Our data (see Table 7) suggest that the rotational motion of the DMSO molecules is very close to the Debye limit, where $\tau_1/\tau_2 = 3$ and rather away from the jump diffusion model.

To our best knowledge, Liu et al. [35] were the first to publish τ_2 values for liquid DMSO-*d*0 at 298 K using the RS, P2 and VG models. They found that all these models underestimate the single molecule second-order reorientation correlation time. Note that the corresponding experimental value, 5.2 ps at 303 K, has been determined by Kovacs et al. [73] assuming an isotropic rotation motion, while the calculated value corresponds to the second-order reorientation ACF of the SO bond unit vector. The assumption of an isotropic rotation motion of the DMSO molecules in the sample was based upon the experimental data concerning the nuclear spin relaxation rates for ^{17}O and ^{33}S. However, this assumption seems to be highly questionable. In addition to this, as discussed earlier in this section, τ_2 values from Rayleigh experiments are indeed expected to be higher than the single molecule relaxation times which are obtained theoretically here and the Raman and NMR values found in the literature. By comparing the various values in Table 6, it is obvious that the value obtained by Bratu et al. [70] from Raman experiments is much higher than all other experimental and theoretical values. For this reason values from Ref. [70] will not be regarded in the remainder of our discussion. Vishnyakov et al. [41] found that the P2 and NPS models give similar τ_2 values which are only slightly higher than those from the OPLS. We note here that the τ_2 experimental values increase in the order: Fox-rigid > GOVG > VG > Bordat > JM4 > Fox-flexible > P2, JM4, NPS, OPLS > RS. When we used the NPS model, the $\tau_{2,a}$ value at 298 K was smaller than the corresponding value obtained using the JM4 model. However, the trend is reversed for the $\tau_{2,b}$ case. Regarding the JM4 model, the τ_2 values increase in the same order as the τ_1 values: *a*-axis (DMSO-*d*6) > *a*-axis (DMSO-*d*0) > *b*-axis (DMSO-*d*6) > *b*-axis (DMSO-*d*0). It should be noted that, in general, the τ_2 values extracted from Raman and NMR measurements are systematically higher than all the theoretical predictions.

3.6. Dipole relaxation times

Using the MD technique, one can calculate the ACF of the total dipole moment, $M(t)$, at time t, $C_M(t) = \langle\vec{M}(0)\vec{M}(t)\rangle/\langle\vec{M}(0)\vec{M}(0)\rangle$. The total dipole moment of the sample is the sum, $\vec{M}(t) = \sum_{i=1}^{N}(\vec{\mu}_p^i + \vec{\mu}_{ind}^i)$, where $\vec{\mu}_p^i(t)$ and $\vec{\mu}_{ind}^i(t)$ denote the permanent and induced dipole moment of the molecule i, respectively. The Debye relaxation time, τ_D can be obtained using the expression $\tau_D = \int_0^\infty C_M(t)\,dt$. Previous MD studies of model polar fluids have shown that using either the Ewald sum method with conducting boundaries or the reaction field method, the results obtained for the dielectric properties are consistent over the whole frequency range (see Ref. [68] and references therein). To obtain accurate data for $\langle M^2(0)\rangle$ and $C_M(t)$ the simulation runs have to be long enough. For this reason in this study 500,000 time steps were used to calculate the ACFs. The τ_μ, τ_D relaxation times results obtained in previous experimental and theoretical data along with results from this work are presented in Table 8.

Skaf and co-workers [29,56,74] presented MD results on the dielectric properties of liquid DMSO-*d*0 using various potential models. In their calculations, the real-space dipolar symmetry projection $h^{110}(r)$ was used to get the k-dependent short-range generalized Kirkwood $g_K^S(r)$ factor. The $k \to 0$ limit of $g_K^S(r)$ provides the shape-independent orientation factor, g_K, and this quantity gives, via the Kirkwood relation, the dielectric constant. These authors also calculated the single-dipole relaxation times, with the dipole moment vector making an angle of 21.6° with the SO bond towards the CH_3 groups. They obtained τ_D relaxation times using the corresponding micro–macro correlation function, $\tau_D = (\varepsilon_0 - 1)/(3y(1+f))\tau_\mu$ and neglecting the dynamical cross correlations between dipoles of distinct molecules [56]. In the previous equation, $y = \rho\mu^2/(9k_B T\varepsilon_0)$ is the dipolar strength, μ the molecular dipole, and ε_0 the system's dielectric constant at zero frequency. Skaf and co-workers calculated single-dipole and Debye relaxation times using the RS, P1, P2, VG and OPLS potential models for the DMSO-*d*0. Skaf's results show that the τ_μ values at 298 K increase in the order P1 > VG > OPLS > P2 > RS. Kurnikova et al. [75] have calculated Debye relaxation times using various models. It is interesting to note that they obtained $\tau_\mu = 7.7$ ps using the VG model at 298 K, a value which is close to the value obtained here, 7.3 ps, but smaller than Skaf [56] using the same model (see Table 8). Kurnikova et al. obtained also very small values, 7.7. ps, using the flex model by Fox and Kollman [43] and even smaller values, 5.2 ps, by using a polarizable model presented in Ref. [75].

The theoretical values can be directly compared with available experimental results obtained by Kaatze et al. [16] at 298 K and time-domain reflectometry measurements by Puranik et al. [76] at various temperatures (see Table 8). It should be noted that these experimental results are in agreement with each other; Kaatze and co-workers obtained $(T, \varepsilon_0, \varepsilon_\infty) = (298\,K, 47.0 \pm 0.6, 3.9 \pm 1)$ and Puranic et al. obtained (288 K, 50.7 ± 3, 4.9 ± 2), (298 K, 48.4 ± 3, 4.5 ± 2), (313 K, 43.3 ± 6, 2.4 ± 4), where ε_∞ is the dielectric constant at infinite frequency. More recently [77], Gabrielian and Markarian used dielectric relaxation spectroscopy and obtained τ_D values in the range 293–333 K for both DMSO and diethylsulfoxide (DESO). Their measurements showed a decrease of τ_D with temperature for DESO. In the case of DMSO, however, no temperature dependence was observed. Thus, the results from Gabrielian et al. were significantly different than those of Kaatze et al. and Puranik et al.

Our results show that the τ_μ values obtained using different potential models increase in the order JM4 > JM9 > P2, OPLS, VG,

Table 8
Experimental and theoretical values of single-dipole (τ_μ), and Debye (τ_D) relaxation times at various temperatures

T (K)	τ_μ (ps)	τ_D (ps)
288[a]		40.0 ± 5
293[b]		20
298[a]		24.6 ± 5
298[c]		21.1 ± 0.2
298[d]	17.6	53
298[e]	8.4	21
298[f]	5.1	13
298[g]	10.7	25
298[h]	10.0	25
298[i]		5.2
298[j]		7.7
298[k]		7.7
298[l]	9.28	
298[m]	7.30	
298[n]	6.88	
298[o]	8.16	
298[p]	8.47	
298[q]	14.05	
298[r]	11.75	
313[a]		14.5 ± 11
313[b]		21.5
323[l]	6.85	
323[m]	6.65	
323[b]		21
323[n]	6.88	
323[o]	2.79	
323[p]	5.38	
323[q]	8.60	
323[r]	6.52	
353[l]	4.16	
353[m]	7.45	
353[n]	10.17	
353[o]	3.88	
353[p]	6.10	
353[q]	6.76	
353[r]	8.41	

[a] Measured in Ref. [16] by recording complex dielectric spectrum using frequency-domain measurements.
[b] Measured in Ref. [77] using dielectric relaxation spectroscopy.
[c] Measured in Ref. [76] by using the time-domain reflectometry (TDR) technique.
[d] (T,τ_μ,τ_D) obtained in Ref. [56] using the P1 model. The τ_D values were calculated from τ_μ using the approximation $\tau_D = \tau_\mu[\varepsilon(0)-1]/[3y(1+f)]$.
[e] (T,τ_μ,τ_D) obtained in Ref. [56] using the P2 model. The τ_D values were calculated from τ_μ using the approximation $\tau_D = \tau_\mu[\varepsilon(0)-1]/[3y(1+f)]$.
[f] (T,τ_μ,τ_D) obtained in Ref. [56] using the RS model. The τ_D values were calculated from τ_μ using the approximation $\tau_D = \tau_\mu[\varepsilon(0)-1]/[3y(1+f)]$.
[g] (T,τ_μ,τ_D) obtained in Ref. [56] using the VG model. The τ_D values were calculated from τ_μ using the approximation $\tau_D = \tau_\mu[\varepsilon(0)-1]/[3y(1+f)]$.
[h] (T,τ_μ,τ_D) obtained in Ref. [56] using the OPLS model. The τ_D values were calculated from τ_μ using the approximation $\tau_D = \tau_\mu[\varepsilon(0)-1]/[3y(1+f)]$.
[i] Obtained in Ref. [75] by using a polarizable model.
[j] Obtained in Ref. [75] by using the VG model.
[k] Obtained in Ref. [75] by using a flexible model by Fox et al. [43].
[l] Calculated from this work using the P2 model.
[m] Calculated from this work using the VG model.
[n] Calculated from this work using the Bordat model.
[o] Calculated from this work using the OPLS model.
[p] Calculated from this work using the NPS model.
[q] Calculated from this work using the JM4 model.
[r] Calculated from this work using the JM9 model.

NPS at 298 K, JM4 > Bordat, P2, VG, JM9 > NPS > OPLS at 323 K, and Bordat > VG > JM4, JM9 > NPS > P2 > OPLS at 353 K. Our new models, JM4 and JM9 seem to perform well at all the temperatures with the JM4 systematically giving higher values than the JM9. Results from this study using the OPLS model at 323 K and 353 K underestimate the experimental measurements. The values of the relaxation times that were produced using the P2 and JM4 models decrease with temperature. However, all the other models show different behaviour. The reason for which the relaxation times do not decrease with temperature in the majority of the models is not clear yet and clearly further work is needed.

It is of great importance, to find simple ways to relate the macroscopic decay of polarization in dielectric systems to a microscopic decay function defined at the molecular level, τ_μ. Two simple models that have been used for a long time are the Glarum–Powles (GP) [78] and the Fatuzzo–Mason (FM) [79] models. The first gives $\tau_D = 3\varepsilon_0/(2\varepsilon_0+\varepsilon_\infty)\tau_\mu$ and the latter $\tau_D = (2\varepsilon_0+\varepsilon_\infty)/(\varepsilon_0+2\varepsilon_\infty)\tau_\mu$. It is quite reassuring that the theoretical results obtained by Skaf [56] agree pretty well with the experimentally determined dielectric relaxation rates. Based on Skaf's results [56], we get τ_D/τ_μ values of 3.01, 2.50, 2.55, 2.34, and 2.5 for the results obtained by using the P1, P2, RS, VG, OPLS, respectively, or on average 2.58. Using the values of the ε_0, ε_∞ obtained by Puranik et al., the GP model gives τ_D/τ_μ values of 1.43, 1.43 and 1.46 at temperatures 288 K, 298 K and 313 K, and the corresponding values from the FM model are 1.76, 1.76 and 1.85. Thus, it is clear that the performance of FM is better. This result is in accordance with similar findings by Svishchev and Kusalik on an MD study of liquid water [80]. These authors used the approximate equations $\tau_D = 3\varepsilon/(2\varepsilon+1)\tau_\mu$ for the GP, and $\tau_D = (2\varepsilon+1)/(\varepsilon+2)\tau_\mu$ for the FM models for liquid water. For the present system and at temperatures between 288 K and 313 K, the FM τ_D/τ_μ values are around 30% lower than the more accurate values obtained by Skaf. Nevertheless, they can serve as a good approximation given the large uncertainties in the measurements and theoretical calculations of these quantities.

3.7. Cage effect and the Stokes–Einstein–Debye relation

We denote as τ_{BC} the time between binary collisions, τ_{res} the residence time that a molecule remains in some equilibrium orientation, τ_S the time associated with structural breakup or rearrangement of a molecular cage, τ_{Or} the measured or calculated reorientational time, and τ_{FL} the time of flight during which a molecule turns through some angle θ. Bartoli and Litovitz [81] identified three limiting cases:

(a) jump diffusion, where $\tau_1/\tau_2 = 1$ and $\tau_{BC} \le \tau_S \le \tau_{Or}$;
(b) free rotation, where $\tau_1/\tau_2 = 1.7$ and $\tau_{Or} \le \tau_{BC} \le \tau_S$;
(c) free diffusion, where $\tau_1/\tau_2 = 3$ and $\tau_{BC} \le \tau_{Or} \le \tau_S$.

In case (a) $\tau_{res} \gg \tau_{FL}$ while in (c) $\tau_{res} \ll \tau_{FL}$. In cases (a) and (c), both small and large angular steps are possible. Note that for liquids: $\tau_{BC} \le \tau_S$. If $\tau_{Or} \le \tau_{BC} \le \tau_S$, the molecule rotates through one or more revolution before it suffers a collision. If $\tau_{BC} \le \tau_{Or} \le \tau_S$, the molecule reorients as a free rotor for a time τ_{BC} and then the angular velocity vector is abruptly changed by a collision. Finally, when $\tau_{BC} \le \tau_S \le \tau_{Or}$, the orientation is 'structure limited' and the molecule is held fixed until structural breakup occurs. In this case, the molecule is free to execute a rotational jump during the time that its environment is 'randomized' and then the molecule is 'trapped' again by the local structure.

The autocorrelation functions of all the linear and angular momenta calculated in this work exhibit a (negative) minimum which can be ascribed to the rebound of a DMSO molecule against the formed cage by its closest neighbours. The cage effect becomes more pronounced at the lowest temperature (298 K) employed in our calculations. Katō et al. [82] used the value of $r_F = \langle F^2\rangle^{1/2}\tau_F(0)/\sqrt{3mk_BT}$ as a criterion for the existence of a translational rebound. In the previous equation, $\langle F^2\rangle$ is the mean squared force acting on a molecule and $\tau_F(0)$ is the time that the force autocorrelation function passes through zero for the first time. According to their criterion, which arises simply from classical mechanics arguments, translational rebound appears whenever $r_F > 1$. The role of this rebound becomes more signifi-

Table 9
Test of the criteria for translational and orientational rebounds

T (K)	$\langle F^2\rangle$ ($\times 10^{-20}$ N^2)	τ_F (0) (ps)	r_F	$\langle T^2\rangle$ ($\times 10^{-40}$ N^2 m^2)	τ_T (0) (ps)	r_T
DMSO-*d*0						
297.5	28.5	0.135	1.80	42.3	0.135	2.53
306.1	28.8	0.144	1.91	42.7	0.136	2.52
310.3	29.2	0.140	1.85	43.2	0.140	2.60
322.5	30.2	0.140	1.85	44.6	0.130	2.40
339.3	30.9	0.142	1.85	45.6	0.133	2.42
350.4	31.7	0.140	1.82	46.7	0.130	2.36
DMSO-*d*6						
296.8	28.5	0.150	1.93	41.8	0.140	2.37
307.5	29.0	0.150	1.92	42.4	0.140	2.34
328.2	30.5	0.144	1.83	44.7	0.144	2.39
354.6	32.1	0.144	1.80	46.7	0.144	2.35

Results for DMSO-*d*0 and DMSO-*d*6 obtained using the JM4 model are presented for various temperatures. See text for details.

cant as r_F becomes higher. Katō et al. [82] used the value of $r_T = \langle T^2\rangle^{1/2}\tau_T(0)/\sqrt{2Ik_BT}$ as a criterion for the existence of a *rotational* rebound. In this case, $\langle T^2\rangle$ is the mean squared torque acting on a molecule and $\tau_T(0)$ is the time that the torque autocorrelation function passes through zero for the first time. Again, the existence of a rebound requires a value of r_T higher than 1. Table 9 summarizes our results using the JM4 model and shows clearly that both criteria are fulfilled for both DMSO-*d*0 and DMSO-*d*6 molecules and for all the temperatures employed. The reversal of linear velocity and angular momentum are in accordance with what one could expect for dense liquids with small moments of inertia and rather anisotropic intermolecular potentials. It is interesting to note that our results show that this quasi-librational motion of the liquid DMSO does not exhibit any significant isotope or temperature dependence.

Many molecular liquids obey the Stokes–Einstein–Debye (SED) relation, which is based on a hydrodynamics model that predicts that the inverse of diffusivity, and the rotational relaxation times are proportional to the ratio of shear viscosity to absolute temperature:

$$1/D = a + b(\eta/T) \tag{5}$$

$$\tau = a' + b'(\eta/T) \tag{6}$$

where a, b, a', b' are constants. The SED equation is in principle applicable to large particles in a medium composed of small molecules and there is yet no proof that it can be applied to small molecules immersed in a solvent composed of molecules of the same size. However, there is some evidence, that the SED law can be more general than is expected purely from its derivation [83,84]. In the limiting case of a sphere under perfect slip boundary conditions, the orientational relaxation time would have no viscosity dependence. The DMSO molecule, however, is not spherical, and when the anisotropy of a molecule is large, a strong coupling between translational, D, and rotational diffusion, Θ, can be observed.

Fig. 9 presents results from the JM4 model on the SED relation for diffusion and for all the rotational relaxation times. It is clear that linearity holds in all cases. We would like to stress that the intercepts and slopes are different for τ_1, τ_2 and $1/D$. In agreement with previous work on CCl_4 by Nakagawa et al. [85] the values of intercept and the slope increase in the order $1/D < \tau_2 < \tau_1$. In our case, the τ_{1a}, τ_{1b} have intercepts of 2.44 ps and 1.49 ps, the τ_{2a}, τ_{2b} have 0.958 ps and 1.00 ps, respectively and the $1/D$ has 1.38×10^8 m^{-2} s. The slopes for τ_{1a}, τ_{1b}, τ_{2a}, τ_{2b} are 9.30, 5.85, 3.52 and 1.95 (in 10^{-11} mPa^{-1} K), respectively and for $1/D$ the slope is 10^{10} m^{-2} mPa^{-1} K. It should also be noted that different rotational axes have different intercepts and slopes. From a microscopic point of view, this means that the molecule has to push different number of molecules out of the way when it reorients about different axes. When it has to push fewer molecules, the rotation about that axis will not be strongly viscosity-dependent.

It is common to correlate the depolarized Rayleigh relaxation time with a SED-type equation [24] $\tau_{Ray} = V\eta/kT + \tau_0$, where V corresponds to the effective hydrodynamic volume for reorientation in the absence of orientation pair correlation, and τ_0 is a constant value that corresponds to the classical free-rotor reorientation time [24,86]. When this equation was applied to our data, V was found less than 5 cm^3 mol^{-1} in all cases, which is considerably smaller than the specific molar volume of pure DMSO (71 cm^3 mol^{-1} at 293 K). This result is not a surprise, since Higashigaki et al. [24] have explained that small molecules in the liquid phase follows slip rather than stick boundary conditions.

4. Conclusions

It should be noted that none of the models examined previously in the literature can accurately reproduce all the properties examined in this study. Our new models perform relatively well at predicting the potential energy and many of the dynamical properties of the DMSO-*d*0 and DMSO-*d*6 systems. The JM4 model performs better than the other four-site model and reproduces the shear viscosity values better than JM9. Thus we recommend the JM4 model for calculations of structure and transport properties of liquid DMSO and its mixtures. We expect, however, that in future studies of hydrogen bonds in mixtures of DMSO, the JM9 model could be useful when one can afford more expensive calculations.

In spite of some inadequacies of the available potential models to describe accurately all the experimental results, the present simulation results revealed many interesting characteristics of the liquid DMSO-*d*0 and DMSO-*d*6. To summarize briefly, the present study clearly shows that there is a significant translation–rotation coupling and the cage effect in the liquid structure results in a translational and rotational rebound. The diffusion coefficients, shear viscosities and rotational relaxation times follow a Stokes–Einstein–Debye relation. Finally, the present work suggests that the Debye relaxation times may show a monotonic dependence on the temperature for the liquid DMSO, verifying the most recent experimental values.

We would like to emphasize on the discrepancy between experimental and theoretical results on the liquid structure. Even a flexible all-atom model [45] fails to reproduce the peak heights of the experiment. Difficulties may have arisen in the experimental determination [6] of the liquid DMSO microscopic structure due to possible contamination with water impurities [87]. In addition to this, there is an intrinsic uncertainty in the experiments due to the large number of overlapping distances in the different pair distribution functions [6] and with the necessity to subtract the intramolecular contribution from the total signal in the neutron diffraction experiments [6]. This resulted in uncertainties in the area of the first peak of around 30% [41]. A redetermination of the experimental distribution function is therefore timely. On the other hand, new calculations with models that take into account polarization and/or different partial charges may provide a better agreement with the available experimental results.

Acknowledgements

We would like to thank Prof. J. Samios (University of Athens) for many useful comments. We are indebted to Prof. Skaf for providing data for Fig. 2 and to Dr. P. Bagot (Heriot-Watt University) for reading an early version of the manuscript. The CPU time of the Computing Centre of the University of Athens (Greece) is also gratefully acknowledged.

References

[1] CRC Handbook of Chemistry and Physics, CRC Press, Boca Raton, FL, 2004.

[2] J.A. Riddick, W.B. Bunger, T.K. Sakand, Organic Solvents Physical Properties and Methods of Purification, John Wiley and Sons, New York, 1986.
[3] D. Martin, A. Weise, H. Niclas, Angew. Chem. Int. Engl. Ed. 6 (1967) 318–334.
[4] R.C. Reid, J.M. Prausnitz, B.E. Poling, The Properties of Gases and Liquids, McGraw-Hill, Singapore, 1987.
[5] B. Kirchner, M. Reither, J. Am. Chem. Soc. 124 (2002) 6206–6215.
[6] A. Luzar, A.K. Soper, D. Chandler, J. Chem. Phys. 99 (1993) 6836–6847.
[7] J.T. Cabral, A. Luzar, J. Teixeira, M.-C. Bellisent-Funel, J. Chem. Phys. 113 (2000) 8736–8745.
[8] J.T. Cabral, A. Luzar, J. Teixeira, M.-C. Bellisent-Funel, Physica B 276–278 (2000) 508–509.
[9] H. Bertagnolli, E. Schultz, P. Chieux, Ber. Bunsenges. Phys. Chem. 93 (1989) 88–95.
[10] S. Itoh, H. Ohtaki, Z. Naturforsch. 42a (1987) 858–862.
[11] H.-C. Chang, J.-C. Jiang, C.-M. Feng, Y.-C. Yang, C.-C. Su, P.-J. Chang, S.H. Lin, J. Chem. Phys. 118 (2003) 1802–1807.
[12] Y. Takasu, Y. Miyashita, Y. Kasai, I. Nishio, J. Phys. Soc. Jpn. 72 (2003) 2665–2670.
[13] T. Tokuhiro, L. Menafra, H.H. Szmant, J. Chem. Phys. 61 (1974) 2275–2282.
[14] E.S. Baker, J. Jonas, J. Phys. Chem. 89 (1985) 1730–1735.
[15] U. Kaatze, M. Brai, F.-D. Scholle, R. Pottel, J. Mol. Liq. 44 (1990) 197–209.
[16] U. Kaatze, R. Pottel, M. Schäfer, J. Phys. Chem. 93 (1989) 5623–5627.
[17] U. Kaatze, V. Lönnecke-Gabel, J. Mol. Liq. 48 (1991) 45–60.
[18] D.N. Shin, J.W. Wijnen, J.B.F.N. Engberts, A. Wakisaka, J. Phys. Chem. B 105 (2001) 6759–6762.
[19] P.P. Wiewior, H. Shirota, E.W. Castner Jr., J. Phys. Chem. 116 (2002) 4643–4654.
[20] N.E. Levinger, B.M. Luther, K.W. Herwig, Abstract of Papers, 220th ACS National Meeting, Washington, DC, 2000.
[21] H.L. Schläfer, W. Schaffernicht, Angew. Chem. 72 (1960) 618–626.
[22] J.M.G. Cowie, P.M. Toporowski, Can. J. Chem. 39 (1961) 2240–2243.
[23] K.J. Packer, D.J. Tomlinson, Trans. Faraday Soc. 1 67 (1971) 1302–1314.
[24] Y. Higashigaki, D.H. Christensen, C.H. Wang, J. Phys. Chem. 85 (1981) 2531–2535, and references there in.
[25] R.T.M. Bicknell, D.B. Davies, K.G. Lawrence, J. Chem. Soc., Faraday Trans. 1 78 (1982) 1595–1601.
[26] E. Cebe, D. Kaltenmeier, H. Hertz, Z. Phys. Chem. (Neue Folge) 140 (1984) 181–189.
[27] M. Holz, X. Mao, D. Seiferling, A. Sacco, J. Chem. Phys. 104 (1996) 669–679.
[28] M. Holz, S.R. Heil, A. Sacco, Phys. Chem. Chem. Phys. 2 (2000) 4740–4742.
[29] M.S. Skaf, S.M. Vechi, J. Chem. Phys. 119 (2003) 2181–2187.
[30] E. Mrazkova, P. Hobza, J. Phys. Chem. A 107 (2003) 1032–1039.
[31] L.M. Jitariu, C. Wilson, D.M. Hirst, J. Mol. Struct. 391 (1997) 111–116.
[32] D.A. McQuarrie, Statistical Mechanics, Harper and Row, New York, 1976.
[33] B.G. Rao, U.C. Singh, J. Am. Chem. Soc. 112 (1990) 3803–3811.
[34] A.K. Soper, A. Luzar, J. Chem. Phys. 97 (1992) 1320–1331.
[35] H. Liu, F. Müller-Plathe, W.F. van Gunsteren, J. Am. Chem. Soc. 117 (1995) 4363–4366.
[36] A. Luzar, D. Chandler, J. Chem. Phys. 98 (1993) 8160–8173.
[37] W.F. van Gusteren, H.J.C. Berendsen, Molecular Simulation (GROMOS) Library Manual, Biomos, Groningen, 1987.
[38] P. Bordat, J. Sacristan, D. Reith, S. Girard, A. Glattli, F. Müller-Plathe, Chem. Phys. Lett. 374 (2003) 201–205.
[39] Y.-J. Zheng, R.L. Ornstein, J. Am. Chem. Soc. 118 (1996) 4175–4180.
[40] W.L. Jorgensen, unpublished results reported in Ref. [39].
[41] A. Vishnyakov, A.P. Lyubartsev, A. Laaksonen, J. Phys. Chem. A 105 (2001) 1702–1710.
[42] D.P. Geerke, C. Oostenbrink, N.F.A. van der Vegt, W.F. van Gunsteren, J. Phys. Chem. B 108 (2004) 1436–1445.
[43] T. Fox, P.A. Kollman, J. Phys. Chem. B 102 (1998) 8070–8079.
[44] I. Benjamin, J. Chem. Phys. 110 (1999) 8070–8079.
[45] M.L. Strader, S.E. Feller, J. Phys. Chem. A 106 (2002) 1074–1080.
[46] S. Senapati, J. Chem. Phys. 117 (2002) 1812–1816.
[47] M. Chalaris, A statistical mechanical computer simulation study of the aprotic (DMSO, DMF) and protic (MeOH, H_2O) solvents, PhD thesis, National and Capodistrian University of Athens, Athens, Greece, 1999.
[48] R. Thomas, C.B. Showemaker, K. Eriks, Acta Crystallogr. 21 (1966) 12–20.
[49] G. Brink, M. Falk, J. Mol. Struct. 5 (1970) 27–30.
[50] M. Chalaris, J. Samios, J. Mol. Liq. 98–99 (2002) 399–409.
[51] R.L. Mancera, M. Chalaris, K. Refson, J. Samios, Phys. Chem. Chem. Phys. 6 (2004) 94–102.
[52] R.L. Mancera, M. Chalaris, J. Samios, J. Mol. Liq. 110 (2004) 147–153.
[53] Y. Zhou, G.H. Miller, Phys. Rev. E 53 (1996) 1587–1601.
[54] S. Marinakis, J. Samios, J. Supercrit. Fluids 34 (2005) 81–89.
[55] T. Douglas, J. Am. Chem. Soc. 70 (1948) 2001–2002.
[56] M.S. Skaf, J. Chem. Phys. 107 (1997) 7996–8003.
[57] G. Liessmann, W. Schmidt, S. Reiffarth, Recommended Thermophysical Data in "Data compilation of the Saechsische Olefinwerke Boehlen", Germany, 1995.
[58] H. Torii, M. Tasumi, Bull. Chem. Soc. Jpn. 68 (1995) 128–134.
[59] T.F. Miller III, D.E. Manolopoulos, J. Chem. Phys. 123 (2005) 154504–154510.
[60] H.L. Robjohns, P.J. Dunlop, Ber. Bunsenges. Phys. Chem. 85 (1981) 655–657.
[61] L. Chen, T. Gross, H.D. Luedemann, Z. Phys. Chem. Munich 214 (2000) 239–251.
[62] G. D' Arrigo, G. Briganti, M. Maccarini, J. Phys. Chem. B 110 (2006) 4612–4620.
[63] K.R. Harris, S. Bair, J. Chem. Eng. Data 52 (2007) 272–278.
[64] J. Barthel, H.-J. Gores, L. Kraml, J. Phys. Chem. 100 (1996) 1283–1287.
[65] T.M. Aminabhavi, V.B. Patil, J. Chem. Eng. Data 43 (1998) 497–503.
[66] A. Sacco, E. Matteoli, J. Solut. Chem. 26 (1997) 527–535.
[67] M.T. Forel, M. Tranquille, Spectrochim. Acta 26A (1970) 1023–1034.
[68] M. Chalaris, J. Samios, J. Chem. Phys. 112 (2000) 8581–8594.
[69] W.T. Huntress Jr., J. Chem. Phys. 48 (1968) 3524–3533.
[70] I. Bratu, T. Iliescu, I. Milea, J. Mol. Liq. 30 (1985) 231–236.
[71] L. Singurel, M. Strat, Acta Phys. Pol. A 47 (1975) 391–396.
[72] P.S. Hubbard, Phys. Rev. 131 (1963) 1155–1165.
[73] H. Kovacs, J. Kowalewski, A. Maliniak, Acta Chem. Scand. Ser. A 41A (1987) 471–479.
[74] M.S. Skaf, Mol. Phys. 90 (1997) 25–34.
[75] M.G. Kurnikova, N. Baladai, D.H. Waldeck, R.D. Coalson, J. Am. Chem. Soc. 120 (1998) 6121–6130.
[76] S.M. Puranik, A.C. Kumbharkhane, S.C. Mehrotra, J. Chem. Soc., Faraday Trans. 88 (1992) 433–435.
[77] L.S. Gabrielian, S.A. Markarian, J. Mol. Liq. 112 (2004) 137–140.
[78] J.G. Powles, J. Chem. Phys. 21 (1953) 633–637.
[79] E. Fatuzzo, P.R. Mason, Proc. Phys. Soc. 90 (1967) 741–750.
[80] I.M. Svishchev, P.G. Kusalik, J. Phys. Chem. 98 (1994) 728–733.
[81] F.J. Bartoli, T.A. Litovitz, J. Chem. Phys. 56 (1972) 413–425.
[82] T. Katō, K. Machida, M. Oobatake, S. Hayashi, J. Chem. Phys. 89 (1988) 3211–3221.
[83] T.J. Chuang, K.B. Eisenthal, Chem. Phys. Lett. 11 (1971) 368–370.
[84] B.J. Alder, D.M. Gass, T.E. Wainwright, J. Chem. Phys. 53 (1970) 3813–3826.
[85] T. Nakagawa, S. Yamanaka, H. Urakawa, K. Kajiwara, H. Maeda, S. Hayashi, J. Mol. Liq. 75 (1998) 127–142.
[86] D.R. Bauer, J.I. Brauman, R. Pecora, J. Am. Chem. Soc. 96 (1974) 6840–6843.
[87] S.E. McLain, A.K. Soper, A. Luzar, J. Chem. Phys. 124 (2006) 074502.
[88] F. Comelli, R. Francesconi, A. Bigi, K. Rubini, J. Chem. Eng. Data 51 (2006) 665–670.
[89] M. Holz, H. Weingaertner, A. Sacco, Ber. Bunsenges. Phys. Chem. 94 (1990) 332–336.